Journal of Computational Physics **179,** 68–94 (2002)
doi:10.1006/jcph.2002.7036

Development of a High-Resolution Nested Air Pollution Model

The Numerical Approach

Lise M. Frohn, Jesper H. Christensen, and Jørgen Brandt

Department of Atmospheric Environment, National Environmental Research Institute, P.O. Box 358, Frederiksborgvej 399, DK-4000 Roskilde, Denmark
E-mail: lmf@dmu.dk

Received February 14, 2001; revised February 22, 2002

A new 3-D model REGINA (REGIonal high resolutioN Air pollution model) is under development at the National Environmental Research Institute (NERI). The model is based on models developed over the past decades at NERI. The goal is to obtain a nested model capable of high-resolution operation. To reach this goal it is necessary to implement sufficiently accurate numerical methods. The model will be applied to studying air pollution phenomena (monitoring, forecasting, and scenarios) over Denmark. In the present paper, the outline of the new model is presented. The numerical methods for transport and chemistry are described. The horizontal transport in the model is solved using an accurate space derivatives algorithm. This method traditionally requires periodic boundary conditions, which are not applicable for nested modeling. Therefore a new method for calculating nonperiodic boundary conditions has been developed. The numerical solution to the chemistry part of the model is obtained from an implementation of a new combination of two existing numerical methods. The results from extensive testing of the numerical solution of the advection and the coupling of the solution of advection and chemistry in the model using Molenkamp–Crowley rotation tests are presented. The same tests have been applied to the model with and without nesting. The results show that the numerical methods are suitable for modeling air pollution levels at high resolution.

Key Words: regional scale air pollution modeling; two-way nesting; rotation test; numerical methods.

CONTENTS

1. *Introduction.*
2. *General description of REGINA.*
3. *Model equations and numerical methods.*

0021-9991/02 $35.00

4. *The first submodel: Three-dimensional advection.*
5. *The fifth submodel: Chemistry.*
6. *Rotation test results.*
7. *Two-way nesting.*
8. *Conclusions and future work.*

1. INTRODUCTION

The modeling of concentrations and depositions of air pollutants requires a large model domain to account for long-range transport. Simultaneously, high resolution in the output is needed to give a good description of the spatio–temporal variability in the concentrations and depositions. Large domains and high resolution are very demanding with respect to both CPU performance and disk space. However, high resolution is normally not necessary over the entire model domain. Therefore a nested grid formulation can be beneficial, since it reduces the computing time needed yet retains the high resolution in the area of interest.

The new model REGINA (REGIonal high resolutioN Air pollution model) is a 3-D model based on the already existing models Danish Eulerian Hemispheric Model [17] (DEHM), Danish Eulerian operational model [8, 9] (DEOM), Danish Rimpuff and Eulerian Accidental release Model [7] (DREAM), and Atmospheric Chemistry and DEPosition model [29] (ACDEP) as well as new methods.

The Danish Eulerian Hemispheric Model is a pseudo-spectral (accurate space derivatives (ASD)) 3-D model covering the majority of the northern hemisphere, developed for calculating the atmospheric transport of sulphur, lead, and mercury to the arctic area. The model has a horizontal resolution of 150×150 km and 18 vertical layers. The Danish Eulerian Operational Model is a pseudo-spectral (accurate space derivatives) model covering the European area, with a horizontal resolution of 50×50 km and three vertical layers. The numerical methods employed in REGINA are further developments from the methods implemented in DEOM and DEHM. The Danish Rimpuff and Eulerian Accidental release Model is a coupled Eulerian and Lagrangian model developed for modeling transport, dispersion, and deposition from accidental releases. The physical parameterization of the planetary boundary layer, the microscale meteorology, and the coupling to MM5 data in REGINA are further developed from the DREAM. The Atmospheric Chemistry and DEPosition model is a Lagrangian transport chemistry model with a domain covering the majority of Europe and a resolution of 30×30 km. The ACDEP model was developed for research on nitrogen deposition to marine waters and contains a relatively detailed description of the nitrogen chemistry. This treatment of nitrogen chemistry will be further developed for future implementation in REGINA.

The REGINA model is an attempt to take into account the very important long-range transportation of air pollutants and the need for high resolution in the calculated concentrations and depositions simultaneously. Furthermore a relatively complex chemical scheme is implemented for the model calculations to be relevant in many different air pollution issues. Within the research field of air pollution modeling, many long-range transport models exist, most of them have relatively complex chemistry, some of them have large domains, and a few of them are nested. REGINA possesses all of these features at the same time. The nested grid formulation makes it possible to obtain high resolution in limited areas, which in theory can be located anywhere in the northern hemisphere (depending on available input data). REGINA can be applied to issues such as forecasting spatial and temporal distribution

of photochemical smog episodes (e.g., O_3), estimation of transboundary air pollution (e.g., SO_2), or calculation of nutrient deposition to sensitive marine or terrestrial ecosystems, in short, forecasting, monitoring, and scenarios. REGINA can be run with the number of nests required to obtain a specific resolution in the output and/or coupled to other models with higher resolution.

The new model is a regional air pollution model, in the sense that it is designed to handle rural and near urban conditions. However, the concentrations of different air pollutants vary greatly with location. As an example the concentration of nitrogen oxides ($NO_X = NO + NO_2$) in urban areas are much higher compared to the concentration in rural areas. NO and NO_2 are closely coupled chemically to ozone (O_3) and this causes large differences in the O_3 concentrations between urban and rural areas. Large gradients are introduced which are difficult to handle numerically. The numerical methods used in a high-resolution air pollution model covering large domains must be flexible enough to solve the coupled chemistry–transport equations in regions of the model domain with very different characteristics, such as urban and rural areas.

In Section 2 a short general description of REGINA is given, followed in Section 3 by a general presentation of the model equations and the numerical methods used to solve them. Section 4 is devoted to the description of the solution of the three-dimensional advection and the new boundary conditions developed for the numerical methods used to solve the horizontal transport. Section 5 deals with the numerical solution of the chemical part of the model. To make sure that the numerical methods used in the model can be applied to different locations, both testing of the model using typical rural concentration levels and testing of the model using typical urban concentration levels have been carried out. The results from extensive testing with the Molenkamp–Crowley rotation test [18, 39], with typical rural concentrations for the model without nesting, are presented in Section 6. The nesting techniques used in the model as well as rotation test results for the model with one nest, both for rural and urban concentrations, are described in Section 7. Finally conclusions and future work are presented in Section 8.

2. GENERAL DESCRIPTION OF REGINA

The domain of REGINA is the northern hemisphere, and the model is constructed using a 3-D Eulerian modeling approach. The meteorological input for the model is calculated using the numerical weather prediction model MM5 [26], which is run in a nested version at the National Environmental Research Institute.

To obtain high-resolution output data, a nested grid formulation is used for the Eulerian model. This is implemented by using a spatial resolution of 150 km $\times$ 150 km over the northern hemisphere (the mother domain), which is projected on a plane using a polar stereographic projection which is true at 60° north. Then each grid cell over the European area is divided horizontally into nine new grid cells, thereby increasing the resolution to 50 km $\times$ 50 km. Further nests are implemented within the first nest. For the northern part of Europe the second nest gives a resolution of approximately 16.67 km $\times$ 16.67 km and the third and currently last nest gives a resolution of approximately 5.56 km $\times$ 5.56 km over Denmark. Each grid contains 96 $\times$ 96 cells. The third nest is not implemented in the calculations performed for the results presented here. In Fig. 1 the domain of the model and the first two nests are shown.

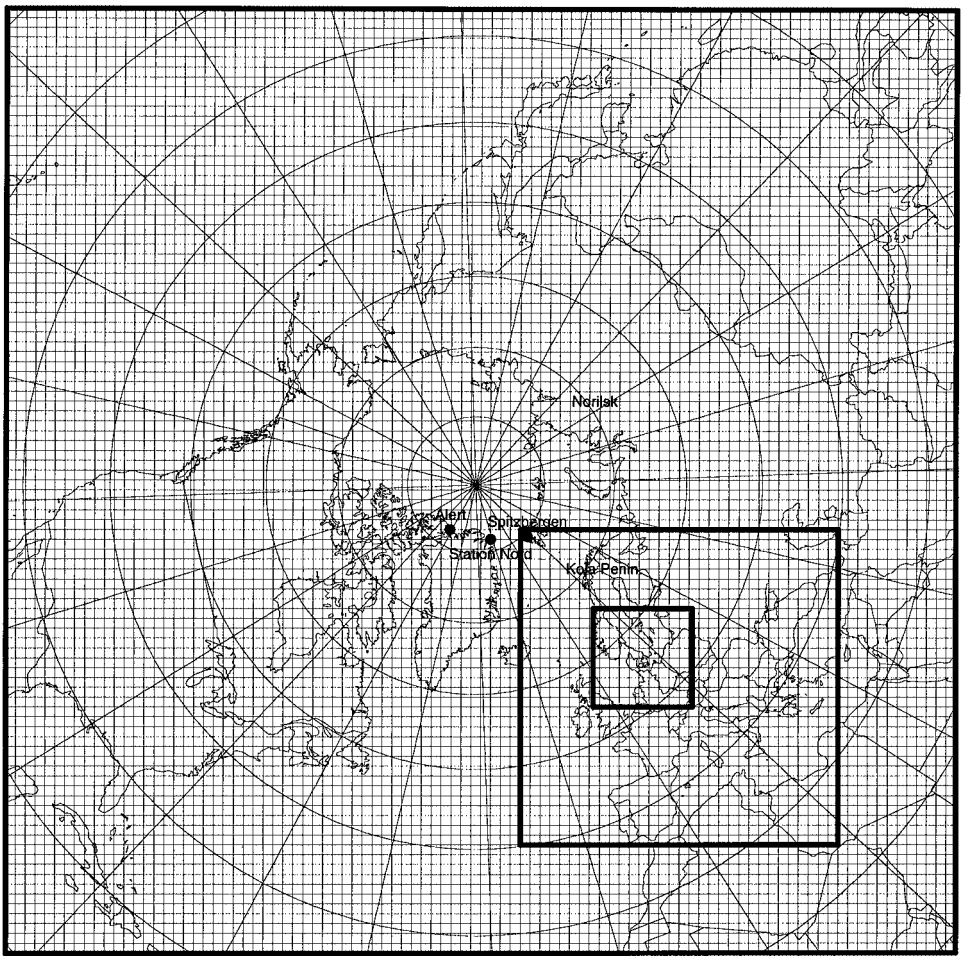

FIG. 1. Model domain for the hemispheric model with two nests.

In the vertical direction a nonequidistant grid with (currently) 18 layers is applied. The vertical grid has the highest resolution close to the ground to describe the processes in the planetary boundary layer, including vertical mixing, dry deposition, and emissions, more accurately. The model domain extends in the vertical direction well up into the stratosphere, with the model top at approximately 17 km.

The chemical scheme used in the model involves 51 chemical species and 113 chemical reactions [22, 46]. It was developed to describe photochemical oxidants with a comprehensive description of the gas phase chemistry and a parameterization of aerosol and liquid phase chemistry. The hydrocarbons are divided into six groups—the first group contains only one species (methane) and the other five groups are represented by five different species (ethane, N-buthane, ethene, propene, and O-xylene). Of the 51 chemical species, 15 are involved in inorganic chemistry, of which the most important are O_3, NO, NO_2, and the radical HO_2. Six species are involved in methane chemistry, six species in ethane chemistry, five species in N-buthane chemistry, four species in ethene chemistry, three species in propene chemistry, seven species in O-xylene chemistry, and five species are involved in isoprene chemistry. There are 28 inorganic reactions, six reactions for aerosol formation,

17 photochemical reactions, and 62 reactions involving methane, hydrocarbons other than methane, and isoprene. The reaction rates, which are most commonly pressure and temperature dependent, are calculated using information which can be obtained from [1, 20]. The photolysis rates for the photochemical reactions are calculated using a method from [32].

3. MODEL EQUATIONS AND NUMERICAL METHODS

The mathematical model in its full length, assuming that the wind velocity fulfills the continuity equation, can be expressed as

$$\frac{\partial c_i}{\partial t} = -\left(u\frac{\partial c_i}{\partial x} + v\frac{\partial c_i}{\partial y} + w\frac{\partial c_i}{\partial z}\right) + K_x\frac{\partial^2 c_i}{\partial x^2} + K_y\frac{\partial^2 c_i}{\partial y^2} + \frac{\partial}{\partial z}\left(K_z\frac{\partial c_i}{\partial z}\right) + E_i(x, y, z, t) + Q_i(c_1, c_2, \ldots, c_q) \quad (i = 1, 2, \ldots, q), \tag{1}$$

where (u, v, w) are wind speed components in the (x, y, z) directions, c_i are the concentrations for the q different species, K_x and K_y are horizontal diffusion coefficients, assumed constant, and K_z is the vertical diffusion coefficient, dependent on space and time coordinates. E_i is the emission of the chemical species i, and Q denotes the chemical reactions.

It is difficult to solve the entire model (Eq. (1)) using a single numerical method due to the very different numerical properties of the processes involved. To remove this difficulty most Eulerian air pollution models are split into submodels which are then treated in turn. Even though a splitting error is introduced, numerical methods, which work especially well for the different submodels can be used, leading to a more efficient and stable numerical scheme [27]. The splitting in REGINA is not implemented in a symmetric fashion, introducing a first-order error. The splitting technique employed follows the widely used approach of [37].

The errors arising from the numerical solution of the different submodels (especially the advection) are in general larger than the error introduced by splitting. For a detailed analysis of the splitting errors for a system, where the chosen splitting time step is much larger than the fastest time scales of the system, and the classical analysis of splitting errors therefore may fail, see [44]. The main conclusions made in [44] are that stiffness of a system has a stabilizing effect for splitting schemes applied to well-partitioned systems and furthermore that the sequence of the operators is crucial; the stiff operator (in this case the chemistry) always has to be treated last in the splitting process. In [35] the splitting errors for advection–diffusion–chemistry problems in air pollution modeling are analyzed to determine the structure and magnitude of the errors and to find out why the splitting technique can work so well. Some of the main conclusions are that the structure of the splitting error is quite complicated, even for simple set-ups, and that it is difficult to determine the magnitude of the splitting error. Furthermore it is concluded that in air pollution models the splitting error will oscillate with a diurnal cycle, approaching zero during night, and not growing beyond bound for evolving time. A more comprehensive analysis of the splitting error is beyond the scope of this paper and the reader is referred to [4, 35, 36, 44].

The model is split into five submodels using a simple splitting procedure based on ideas from [37]. The five submodels are:

- Submodel 1: Three-dimensional advection

$$\frac{\partial c_i^1}{\partial t} = -u\frac{\partial c_i^1}{\partial x} - v\frac{\partial c_i^1}{\partial y} - w\frac{\partial c_i^1}{\partial z}. \tag{2}$$

- Submodels 2–4: Diffusion

$$\frac{\partial c_i^2}{\partial t} = K_x \frac{\partial^2 c_i^2}{\partial x^2}$$
$$\frac{\partial c_i^3}{\partial t} = K_y \frac{\partial^2 c_i^3}{\partial y^2}$$
$$\frac{\partial c_i^4}{\partial t} = \frac{\partial}{\partial z}\left(K_z \frac{\partial c_i^4}{\partial z}\right). \tag{3}$$

- Submodel 5: Chemistry and emissions

$$\frac{dc_i^5}{dt} = Q_i\left(c_1^5, c_2^5, \ldots, c_q^5\right) + E_i. \tag{4}$$

In the mathematical formulation of the solution of the vertical diffusion, the term for the downward flux in the lowest vertical layer is given as the dry deposition velocity multiplied with the surface concentration. Submodel 1, three-dimensional advection, is solved using an accurate space derivatives scheme for the horizontal advection, combined with a finite elements scheme for the vertical advection. The temporal integration of advection is carried out using a Taylor series expansion to third order. See Section 4 for details. The submodels 2–4, diffusion, are solved using a finite elements scheme for the spatial discretization and the θ method [33] for the temporal integration. The finite elements method is used for solving both the horizontal and the vertical diffusion. The diffusion process is highly parameterized in the model, since K-theory of first order is used for the diffusion and the diffusion coefficients for the horizontal diffusion are assumed constant. The finite elements method is capable of working with nonequidistant grids, which is an advantage for the vertical diffusion. The time integration of the diffusion needs to be carried out using a very stable numerical method. This is due to the fact that the diffusion, which can be quite strong, for example, under convective conditions, is also subject to stability criteria. In this case the θ method is chosen because it is an implicit method, and therefore more stable. The solution of the diffusion submodels will not be discussed in this paper but the reader is referred to [16, 17] for comprehensive treatments. Submodel 5, chemistry and emissions, is solved using a combination of the Euler backward iterative method and a two-step method; see Section 5 for details.

4. THE FIRST SUBMODEL: THREE-DIMENSIONAL ADVECTION

When solving the advection equation (2) numerically, the numerical diffusion degrades the computed solution. To overcome this problem many different numerical advection schemes have been developed. In [31] it is shown that errors in the solution of the advection submodel are amplified during the chemistry submodel due to the highly nonlinear nature of the chemistry.

If a low-order numerical scheme is used for solving the advection, the result is a solution with little oscillations; however, the accuracy is not very good. Using a high-order numerical scheme gives high accuracy, but the solution is characterized by computational noise and oscillations especially in areas with sharp gradients. This oscillatory noise increases and propagates to other grid points and this can result in negative concentrations corresponding to "negative mass," which is not physically meaningful. To overcome these problems different

filtering techniques are used. The filters remove the computational noise after each advection step as well as the negative concentrations, and the effect is that the filtered solution retains the high accuracy of the high-order numerical scheme yet gives a physically acceptable distribution with little oscillations and a positive concentration distribution.

In [19] it is indicated that the method of accurate space derivatives [25], which is used for solving the horizontal advection in REGINA, is one of the most accurate methods for solving the advection equation. Combined with the Forester filter [24] it produces very accurate results. The ASD method is not positive definite by nature. To make sure that no negative concentrations appear a Bartnicki filter [2] is applied to the concentration distribution calculated with the ASD method. The Bartnicki filter redistributes the possible negative concentration values. For more details on the filtering see Section 4.3.

Other air pollution models (the variable-grid urban airshed model [43] (UAM-V), the regional acid deposition model [13] (RADM), the EURAD-CTM system [12, 27], the REM3 system [41, 45], the NILU system [22, 23], the multiscale atmospheric transport and chemistry model [34, 42] (MATCH), and the EUROPOLLUX system [38]) exist with and without nesting, covering different domains and with resolutions up to a few kilometres or less. Few of these models are hemispheric and none of the models employ spectral methods for solving the advection.

The method of finite differences is frequently used in numerical weather prediction models; however it is not used in state-of-the-art air pollution modeling, due to the low accuracy, which is not sufficient for a model which has to handle sharp gradients in air pollution concentration distributions. The method of finite elements has earlier been used to some extent; however, the Bott scheme [10, 11] is now one of the most frequently used advection schemes in air pollution modeling. The majority of the existing nested models have implemented the Bott scheme and some employ versions of an upwind scheme with telescopic grids [47]. The Bott scheme is a flux scheme and as such not concentration conserving [21]. In most implementations this problem is taken care of by the rather nonphysical approach of adjusting wind fields to obtain concentration conservation. The upwind scheme has the problem of introducing large artificial diffusion. Numerical tests have shown that the accurate space derivatives scheme introduces fewer oscillations and hence performs better than the finite elements scheme; see [6, 15].

The three-dimensional advection equation is integrated with respect to time using a third-order Taylor series method. The $\frac{\partial c}{\partial x}$ and $\frac{\partial c}{\partial y}$ terms of the advection equation (2) are determined using the ASD method and the $\frac{\partial c}{\partial z}$ terms are determined using a finite-element method.

4.1. Discretization in Time

The discretization of the advection equation in time is carried out using a Taylor series expansion to third order [3]:

$$c(t+\Delta t) \simeq \sum_{n=0}^{3} \frac{1}{n!}\frac{\partial^n c}{\partial t^n}\cdot(\Delta t)^n$$
$$= c(t) + \frac{1}{2}c'(t)\Delta t + \frac{1}{6}c''(t)(\Delta t)^2 + \frac{1}{24}c'''(t)(\Delta t)^3. \quad (5)$$

This type of time discretization is very similar to what is done in Lax–Wendroff style finite difference advection methods. The Courant–Friedrich–Levy (CFL) stability criterion

associated with the method of accurate space derivatives for a third-order Taylor series expansion is 0.5, as derived by [2],

$$u\frac{\Delta t}{\Delta x} < 0.5, \quad v\frac{\Delta t}{\Delta y} < 0.5, \quad w\frac{\Delta t}{\Delta z} < 0.5, \tag{6}$$

where Δx, Δy, and Δz are the resolutions in the x, y, and z direction, Δt is the temporal resolution and u is the maximum windspeed in the x direction. For $c(t)$ discretized values $\tilde{c}$ are used. $c'(t)$ is calculated using spatial derivatives:

$$c'(t) = -u\frac{\partial c}{\partial x} - v\frac{\partial c}{\partial y} - w\frac{\partial c}{\partial z}. \tag{7}$$

$$= \bar{v} \cdot \bar{\nabla} c. \tag{8}$$

The second derivative ($c''(t)$) and the third derivative ($c'''(t)$) are calculated using a similar procedure,

$$c'' = \bar{v} \cdot \bar{\nabla} c' \tag{9}$$

$$c''' = \bar{v} \cdot \bar{\nabla} c'' \tag{10}$$

and the first, second, and third derivatives of the concentration field are then discretized.

4.2. Discretization in Space

The domain of the model is discretized using $N = 96$ grid points uniformly spaced in the x and y directions with spacing equal to Δx and Δy. The N grid points in the x direction are denoted $x_1, \ldots, x_N$, where $x_N - x_1 = (N-1)\Delta x$.

The concentrations at every grid point, $\tilde{c}(x_i)$ are calculated with the aid of a continuous function c:

$$\begin{aligned} \tilde{c}(x_1) &= c(0) \\ \tilde{c}(x_2) &= c(\Delta x) \\ &\vdots \quad \vdots \\ \tilde{c}(x_N) &= c((N-1)\cdot\Delta x). \end{aligned} \tag{11}$$

The formulation of the continuous function c is new. It consists of a cosine function, $P(x)$, to account for the variation of the field on the boundary (see Section 4.4) and a Fourier expansion, $F(x)$, to describe the general variation of the field. Considering the x direction only, $c(x)$ is given by (x with no indices denotes a continuous variable),

$$c(x) = P(x) + F(x); \quad x \in [0, (N-1)\cdot\Delta x], \tag{12}$$

where

$$P(x) = \left(\frac{c(x_1) - c(x_N)}{2}\right)\cos(\kappa x) + \left(\frac{c(x_1) + c(x_N)}{2}\right) \tag{13}$$

and

$$F(x) = \sum_n (a_n \cos(2n\kappa x) + b_n \sin(2n\kappa x)), \tag{14}$$

where $\kappa = \frac{\pi}{N\Delta x}$. Note that for $x = x_1$ and $x = x_N$ the function $P(x)$ gives $c(x_1)$ and $c(x_N)$ in agreement with the values on the boundaries. The Fourier coefficients a_n and b_n are determined from the values of the concentration field in the grid points such that

$$c(x = x_i) = \tilde{c}(x_i) \tag{15}$$

for all i.

The continuous function $c(x)$ is differentiated with respect to x to obtain the spatial derivatives of the concentration field:

$$\begin{aligned}\frac{\partial c}{\partial x}(x) &= \frac{\partial P}{\partial x}(x) + \frac{\partial F}{\partial x}(x) \\ &= -\kappa\left(\frac{c(x_1) - c(x_N)}{2}\right)\sin(\kappa x) + \sum_n(-a_n(2n\kappa)\sin(2n\kappa x) \\ &\quad + b_n(2n\kappa)\cos(2n\kappa x)).\end{aligned} \tag{16}$$

This function is then discretized to obtain derivatives of $\tilde{c}_i$: $\frac{\partial \tilde{c}}{\partial x}$. The same procedure is applied to the y direction to obtain $\frac{\partial \tilde{c}}{\partial y}$ values.

The method of finite elements involving linear shape functions [40] is used for solving the vertical advection because it is reasonably accurate and computationally fast. It is also applicable to nonequidistant grids, as used in the vertical discretization of the model. The uncertainty in the vertical wind speed components is in general an order of magnitude larger than the uncertainty in the horizontal wind speed components and therefore it is not necessary to implement a very accurate numerical scheme for the solution of the vertical advection. The $\frac{\partial \tilde{c}}{\partial z}$ values are obtained using a Galerkin implementation of the finite elements scheme [40].

For x and y held constant, the advection equation becomes

$$\left.\frac{\partial c}{\partial t}\right|_{x,y=\text{constant}} = -w\frac{\partial c}{\partial z}. \tag{17}$$

The vertical domain of the model is discretized using $N_z = 18$ grid points in the z direction (with nonequidistant spacing Δz). The N_z grid points in the z direction are denoted $z_1, \ldots, z_{N_z}$. The concentration at every grid point is denoted by $\tilde{c}(z_i, t)$ and the value of the vertical windspeed at every grid point is denoted by $\tilde{w}(z_i, t)$, where $i = 1, \ldots, N_z$.

The linear shape functions are continuous functions of the continuous variable z:

$$e_i(z) = \begin{cases} \frac{(z - z_{i-1})}{(z_i - z_{i-1})} & \text{if } z_{i-1} < z \le z_i \\ \frac{(z_{i+1} - z)}{(z_{i+1} - z_i)} & \text{if } z_i < z \le z_{i+1} \\ 0 & \text{otherwise.} \end{cases} \tag{18}$$

Two continuous functions describing the concentrations and the vertical wind speeds are constructed using the values at the grid points $\tilde{c}$ and $\tilde{w}$ and the linear shape functions

$$c(z,\ t) \approx \sum_k \tilde{c}(z_k,\ t)e_k(z) \tag{19}$$

and

$$w(z,t) \approx \sum_j \tilde{w}(z_j,\ t)e_j(z), \tag{20}$$

where $k,\ j = 1, \ldots, N_z$. The above expressions for c and w are substituted into Eq. (17) to give

$$\sum_k \frac{\partial \tilde{c}(z_k,\ t)}{\partial t} e_k(z) = \sum_j \sum_k -\tilde{w}(z_j,\ t)e_j(z)\tilde{c}(z_k,\ t)\frac{\partial e_k(z)}{\partial z}. \tag{21}$$

To fulfill the Galerkin orthogonality criteria, the above equation is multiplied by $e_i(z)$ and the result is integrated over the vertical variable

$$\sum_k \frac{\partial \tilde{c}(z_k,t)}{\partial t} \int_z e_k(z)e_i(z)\,dz \tag{22}$$

$$= \sum_j \sum_k -\tilde{w}(z_j,t)\tilde{c}(z_k,t) \int_z e_j(z)e_i(z)\frac{\partial e_k(z)}{\partial z}\,dz. \tag{23}$$

After integration over the continuous variables a system of ODEs is obtained. For every interior point, the system can be expressed as

$$\frac{1}{6}\frac{d}{dt}(\Delta z_{i-1}\tilde{c}(z_{i-1},t) + 2(\Delta z_{i-1} + \Delta z_i)\tilde{c}(z_i,t) + \Delta z_i \tilde{c}(z_{i+1},t))$$
$$= \frac{1}{6}((\tilde{w}_{i-1} + 2\tilde{w}_i)\tilde{c}(z_{i-1},t) + (\tilde{w}_{i+1} - \tilde{w}_{i-1})\tilde{c}(z_i,t) - (\tilde{w}_{i+1} + 2\tilde{w}_i)\tilde{c}(z_{i+1},t)), \tag{24}$$

where $\Delta z_n = z_{n+1} - z_n$; $n = 1, \ldots, N_z - 1$ and the explicit time and spatial dependency of $\tilde{w}$ has been omitted for brevity, such that $\tilde{w}_i = \tilde{w}(z_i, t)$.

The boundary conditions for the finite elements method are given as follows. For the lowest limit (close to the surface) only half of the linear shape function is used. This gives the following ODE:

$$\frac{1}{6}\frac{d}{dt}(2\Delta z_1\tilde{c}(z_1,t) + \Delta z_1\tilde{c}(z_2,t)) = \frac{1}{6}((\tilde{w}_2 + 2\tilde{w}_1)\tilde{c}(z_1,t) - \tilde{w}_1\tilde{c}(z_2,t)). \tag{25}$$

For the upper limit the following conditions are used for the concentrations and vertical wind speeds

$$\tilde{c}(z_{N_z+1},t) = c_{back} \tag{26}$$

and

$$\tilde{w}_{N_z+1} = 0, \tag{27}$$

which gives the expression

$$\frac{1}{6}\frac{d}{dt}\big(\Delta z_{N_z-1}\tilde{c}\big(z_{N_z-1},t\big) + 2\big(\Delta z_{N_z-1} + \Delta z_{N_z}\big)\tilde{c}\big(z_{N_z},t\big) + \Delta z_{N_z}c_{back}\big)$$
$$= \frac{1}{6}\big(\big(\tilde{w}_{N_z-1} + 2\tilde{w}_{N_z}\big)\tilde{c}\big(z_{N_z-1},t\big) - \tilde{w}_{N_z-1}\tilde{c}\big(z_{N_z},t\big) - 2\tilde{w}_{N_z}c_{back}\big) \tag{28}$$

as the ODE to be solved for the upper boundary.

The total system of ODEs can be expressed as

$$A\frac{d\tilde{c}}{dt} = D\tilde{c}. \tag{29}$$

Both A and D are tridiagonal matrices, given by

$$A = \begin{bmatrix} 2\Delta z_1 & \Delta z_1 & 0 & \dots & 0 & 0 \\ \Delta z_1 & 2(\Delta z_1 + \Delta z_2) & \Delta z_2 & \dots & 0 & 0 \\ \vdots & \vdots & \vdots & \vdots & \vdots & \vdots \\ 0 & 0 & 0 & \dots & \Delta z_{N_z-1} & 2\Delta z_{N_z-1} \end{bmatrix} \tag{30}$$

and

$$D = \begin{bmatrix} \tilde{w}_2 + 2\tilde{w}_1 & -(\tilde{w}_2 + 2\tilde{w}_1) & 0 & \dots & 0 & 0 & 0 \\ 2\tilde{w}_2 + \tilde{w}_1 & \tilde{w}_3 - \tilde{w}_1 & -(2\tilde{w}_2 + \tilde{w}_3) & \dots & 0 & 0 & 0 \\ \vdots & \vdots & \vdots & \vdots & \vdots & \vdots & \vdots \\ 0 & 0 & 0 & \dots & 2\tilde{w}_{N_z} + \tilde{w}_{N_z-1} & -\tilde{w}_{N_z-1} & -2\tilde{w}_{N_z} \end{bmatrix}. \tag{31}$$

Equation (29) is multiplied with A^{-1} to obtain an explicit expression for $\tilde{w}\frac{\partial\tilde{c}}{\partial z}$. This expression is inserted in the advection equation (2), which can then be solved with respect to time.

4.3. Filtering

The Forester filter [24] is used to smooth out spurious oscillations in the calculated concentration field. It is based on the introduction of local diffusion. It uses four parameters, n, m, K, and μ. The parameters n and m determine the noise wavelength, $2n$ is the number of mesh intervals local extrema are separated by using the local diffusion. K is the number of iterations to be carried out, and μ is a dimensionless diffusion coefficient. The parameters are problem dependent and must be determined using an empirical approach. The filter can be described using the iterative scheme

$$C_i^{k+1} = C_i^k + \frac{\mu}{2}[(C_{i+1} - C_i)(\psi_i + \psi_{i+1}) - (C_i - C_{i-1})(\psi_i + \psi_{i-1})]^k, \tag{32}$$

where C_i^{k+1} is the value of C_i after k iterations of the filter. The values of ψ are either 0 or 1 and determine the points at which smoothing occurs. They are computed from the filter parameters m and n. For further details the reader is referred to [24]. In the present study n equals 2, $m = 1$, $K = 1$, and $\mu = 0.2 \cdot 2u \cdot \frac{\Delta t}{\Delta x}$. In the present implementation of the Forester filter μ is dependent on the CFL number (the CFL number in the x direction for Forester filtering in the x direction, etc.) in the corresponding grid cell to decrease numerical diffusion for low CFL numbers. The Forester filter is not applied to the boundary rows and columns of the model domain (and the nested domains) since it tends to create gradients at the boundaries.

The Bartnicki filter [2] is used to remove negative (nonphysical) values from the concentration distribution. A very simple strategy is used for redistributing the negative concentrations, in which all the negative concentrations are converted to mass and added. Equal

amounts are then subtracted from all the positive (mass) values in the distribution. Zero value concentrations are not modified and if all concentrations in the distribution are positive the filter does not affect the distribution. The total mass, which is subtracted from the distribution, equals the total initial negative mass. The filter conserves the total mass, preserves the shape of the distribution, and preserves the distribution maxima. Two iterations of the filter have in previous studies [3, 19] been found sufficient for removing all negative concentrations.

4.4. Horizontal Boundary Concentrations

The ASD method in its original form has an unwanted requirement of periodic boundary conditions, which can be achieved, but in a somewhat artificial manner. The cosine function $P(x)$, as described in Section 4.2, is introduced to avoid the periodic boundary condition. Nonperiodic boundary conditions are necessary, especially for the nested areas to avoid nonphysical sharp gradients on the boundaries. The new way of calculating boundary concentrations is especially well suited for nested models.

For the boundary concentrations in the solution of the horizontal advection a finite differences scheme is used to calculate the new concentrations. The following procedure is used depending on the direction of the flow across the boundary. c_{back} denotes the background concentration used on the boundaries when the model is initialized.

As an example consider the boundary of the domain at $x = 1$. For inflow a boundary concentration c_{bound} is determined as

$$c_{bound} = u\frac{\Delta t}{\Delta x} \times c_{back} + \left(1 - u\frac{\Delta t}{\Delta x}\right) \times c(x_2). \tag{33}$$

For outflow c_{bound} is given by

$$c_{bound} = -u\frac{\Delta t}{\Delta x}c(x_3) + \left(1 + u\frac{\Delta t}{\Delta x}\right) \times c(x_2). \tag{34}$$

Finally the concentrations for the grid cells with $x = x_1, x_2$ are set to

$$c(x_1) = c(x_2) = c_{bound}. \tag{35}$$

The same procedure is carried out for the other boundary grid points ($x = x_{N-1}, x_N$) and for the y direction. For $c(x_1)$, $c(x_2)$, $c(x_{N-1})$, and $c(x_N)$ (and corresponding points for the y direction) the derivatives with respect to x (y) are set to zero.

5. THE FIFTH SUBMODEL: CHEMISTRY

The numerical solution to the fifth submodel is obtained using two different numerical methods, the Euler backward iterative or EBI method [28] and the two-step method [48]. For a given set of error tolerances, the two-step method runs with the largest time step compared to the EBI method, indicating that it is the most accurate of the two. However, the two-step method needs two initial concentration fields, and therefore the EBI method is used in the first chemistry step to provide the two fields that are needed.

Expressing the chemistry term in Eq. (4) as a sum of production and loss terms, the equation becomes

$$\frac{dc}{dt} = P - Lc. \tag{36}$$

P is the production term (including emissions) and L is the loss term due to chemistry. The new concentration field, as calculated using the EBI method, is given by

$$c_{n+1} = \frac{c_n + P(c)\Delta t}{1 + \Delta t L(c)}. \tag{37}$$

This solution is iterated twice to provide the two initial concentration fields for the two-step method. The time step is set to the default values of 100 s (daytime) and 300 s (nighttime). After each iteration a thorough error check is carried out, calculating the mean error for each chemical species. It is then checked that the change in concentration for every species is within a certain limit of tolerance. If this is not the case the time step is adjusted according to the size of the error. For details on the error calculation procedure see [48].

The solution of the chemistry submodel using the two-step method is given by

$$c_{n+1} = \frac{\frac{(\epsilon+1)^2 c_n - c_{n-1}}{\epsilon^2 + 2\epsilon} + \gamma \cdot \Delta t P}{1 + \gamma \Delta t L}, \tag{38}$$

where ϵ and γ are given by

$$\epsilon = \frac{\Delta t_{old}}{\Delta t_{new}} = \frac{t_n - t_{n-1}}{t_{n+1} - t_n} \tag{39}$$

and

$$\gamma = \frac{\epsilon + 1}{\epsilon + 2}. \tag{40}$$

Two iterations are carried out for every calculation of new concentrations. The calculation of production and loss terms is made using a Gauss–Seidel type iteration process [48] in which the calculated production and loss term of a species i is taken into account in the following calculation for species j (with chemistry involving species i). This is done to give production and loss terms which are based on the concentration field under calculation.

A maximum error is calculated for every chemical species after each time step. The error check is again based on whether the change in concentration of a certain species is within a given tolerance. The new time step for the chemistry is adjusted according to the size of the errors. For details on the error calculation procedure see [48].

6. ROTATION TEST RESULTS

To test the numerical solution of advection and the coupling to chemistry, the Molenkamp–Crowley rotation test [18, 39] has been applied. The Molenkamp–Crowley rotation test is a very challenging test for evaluating the numerical solution of advection as well as coupling

of different processes (advection and chemistry). The rotation test is widely used in air pollution modeling, see, e.g., [5, 14–16, 19, 30, 31, 49, chap. 4].

The purpose of performing the rotation tests is three-fold. First the performance of the numerical solution for advection is tested. This is done to make sure that the numerical method is not introducing unrealistic oscillations in the calculated concentration distribution. The advection algorithm must be able to solve the advection problem with as small errors as possible. The rotation test is very well suited for this and is applied to the model without nesting as well as nested versions.

Secondly if an advection algorithm has been tested and approved and furthermore a carefully tested chemical algorithm has been chosen, then the question to be answered by the rotation test results is whether the combination of these two algorithms also performs well. As documented in [5, 6] this is not always the case. In some cases the advection algorithm introduces small oscillations which are amplified in the solution of the nonlinear chemistry. The rotation test reveals any problems that might occur in the coupling between the two algorithms and for this reason it is used for testing the coupling between advection and chemistry. The rotation test is in this case applied to the model with typical rural as well as typical urban conditions, since the (final) model will be applied to both rural and urban areas.

Thirdly the rotation test is used to evaluate the performance of adding a filter—the Forester filter—to the solution of the advection. A very important part of solving the advection in a model is the application of filters. This is because the presence of a filter can affect the numerical results strongly. The Forester filter has earlier been documented to be very accurate in combination with the ASD method [19], and it is tested whether this still applies for the modified ASD method.

The model set-up for the rotation test includes the same chemical scheme with 51 species as the model set-up for the regional model [22, 46]. The discretization and number of grid points are the same; however, no topography, no emissions, and no depositions are included. The test is prepared such that one rotation takes approximately 24 h. There is no diffusion submodel in the test, since this would make it more difficult to determine the amount of artificial diffusion in the advection scheme. The wind velocities are defined so that the wind trajectories are concentric circles with a common center. Furthermore the angular velocity is constant. After a certain amount of time corresponding to one full rotation around the common center (in this case 24 h) a given distribution of the concentrations (in this case in the shape of a concentric cone) will be back at the starting point [6].

Several different versions of the test have been run. The first test is running the model without chemistry (advection only). After a full rotation the shape of the cone should be similar to the initial distribution, if the numerical errors are small. In the second test the model is run without advection to give a final distribution when chemistry only is applied. When the model applying both advection and chemistry is run the results after a full rotation should be similar to the results from the chemistry only test. The same test is also run with the Forester filter (and advection and chemistry) to observe the influence of the filter on the numerical solution. Furthermore these tests are also carried out for the model with one and two nests.

The species chosen for the test are NO_2 and O_3. NO_2 is a primary pollutant with direct emission sources (combustion processes) and acts among other things as a precursor for O_3. O_3 is a secondary chemical species meaning that it has no direct emission source. It is produced from reactions between other primary pollutants. For this reason the concentration field for O_3 is initially set to a background value, constant throughout the field. When the chemical algorithm is applied O_3 is produced and after a time period a cone of O_3 is formed.

TABLE I
Initial Maximum Concentrations of NO, NO_2, and O_3 for Rural and Urban Conditions

Conditions	NO (ppb)	NO_2 (ppb)	O_3 (ppb)
Rural	1	10	20
Urban	100	5	20

For O_3 it is not meaningful to discuss the results of the rotation test with advection only; however, the results of combining the advection and chemistry solvers can be compared to the results of applying the chemistry solver alone. O_3 is especially interesting because the chemistry introduces very sharp gradients in the O_3 concentration distribution. The initial maximum concentration values for rural and urban conditions are given in Table I.

Results for NO_2 and O_3 for the hemispheric model without nesting can be seen in Figs. 2 and 3. The initial concentrations correspond to typical rural concentration levels.

In Table II the maximum and minimum values of the concentration field after one full rotation are shown for the rotation test set-ups without nesting and rural conditions.

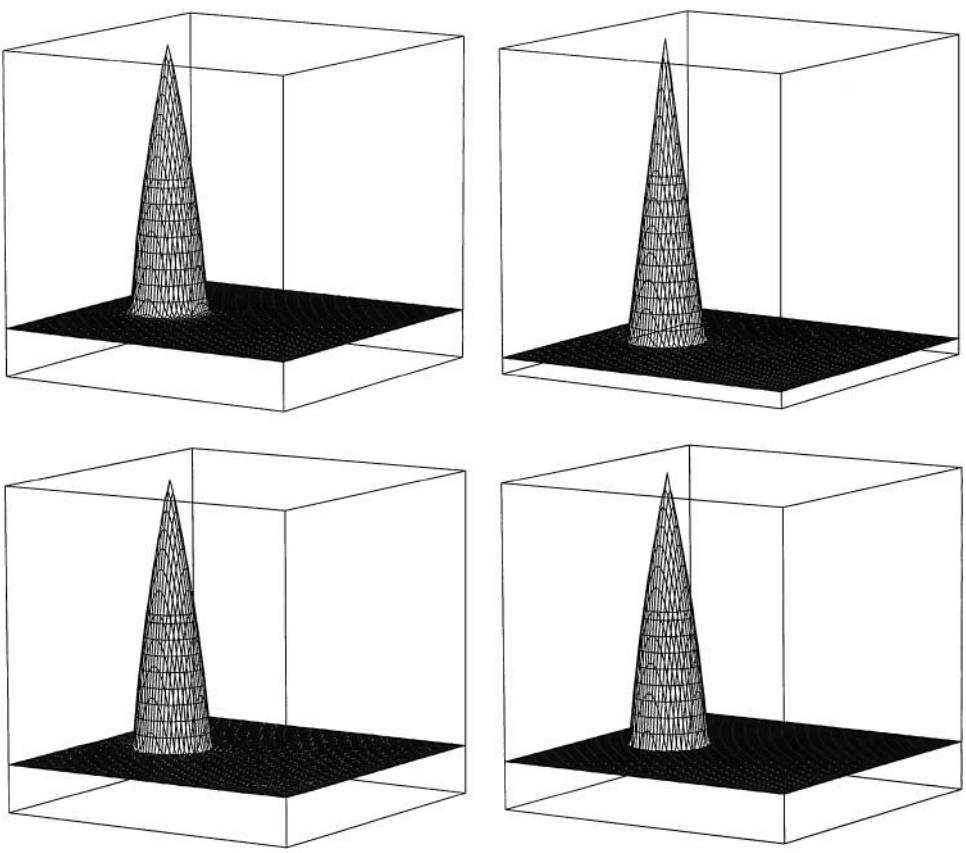

FIG. 2. Rotation test for NO_2 without nesting, rural conditions. The results are given for advection only (upper right), chemistry only (lower right), advection and chemistry combined (lower left), and advection, chemistry, and Forester filter combined (upper left).

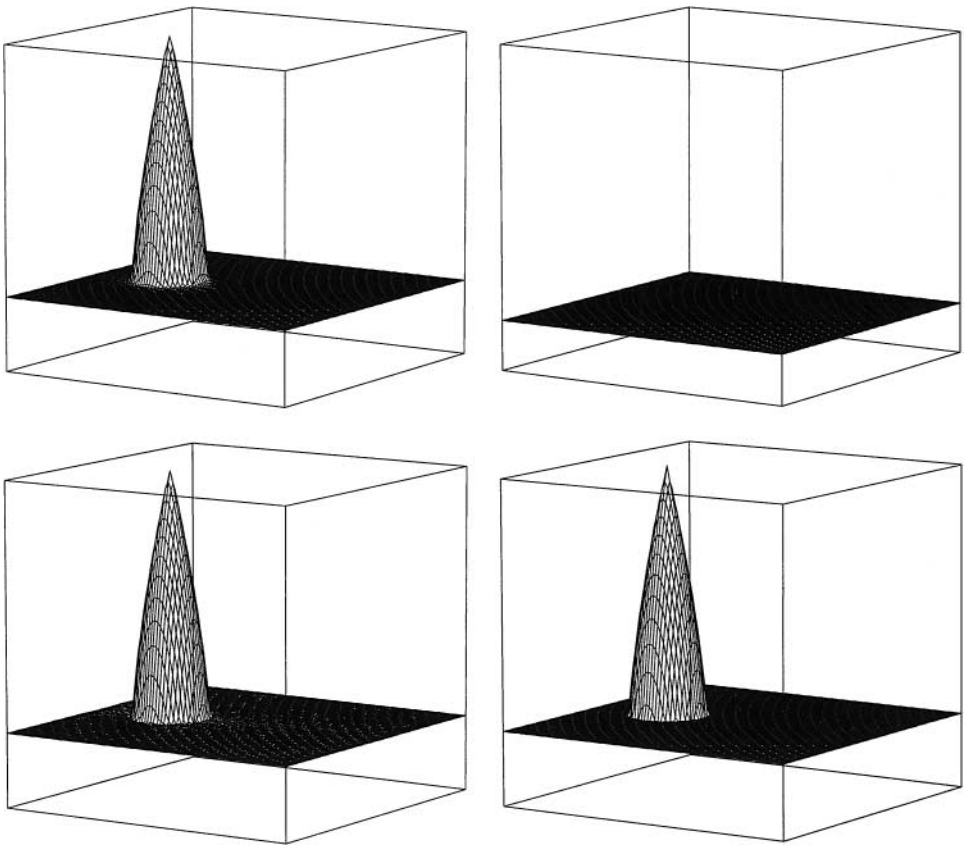

FIG. 3. Rotation test for O_3 without nesting, rural conditions. The results are given for advection only (upper right), chemistry only (lower right), advection and chemistry combined (lower left), and advection, chemistry, and Forester filter combined (upper left).

In the upper right part of the figures the result of applying advection only is shown. The result for NO_2 is very close to the initial concentrations (not shown here) and for O_3 the initial concentrations are set to a background value. In the lower right part of the figures the result is shown when chemistry only is applied.

The chemistry is highly nonlinear and very sharp gradients can appear because of this nonlinearity. These sharp gradients put high demands on the numerical scheme used for

TABLE II

Maximum and Minimum Values of the Concentrations after One Full Rotation for the Model Set-Ups Chemistry Only, Advection Plus Chemistry, and Advection, Chemistry Plus Forester Filter

		Chemistry only		Advection, chemistry		Advection, chemistry, Forester	
Figure	Species	Max.	Min.	Max.	Min.	Max.	Min.
2	NO_2	0.65	0.10	0.65	0.09	0.65	0.10
3	O_3	134.00	30.86	134.00	29.64	134.00	30.86

Notes. The initial concentrations correspond to rural conditions. All values are in ppb.

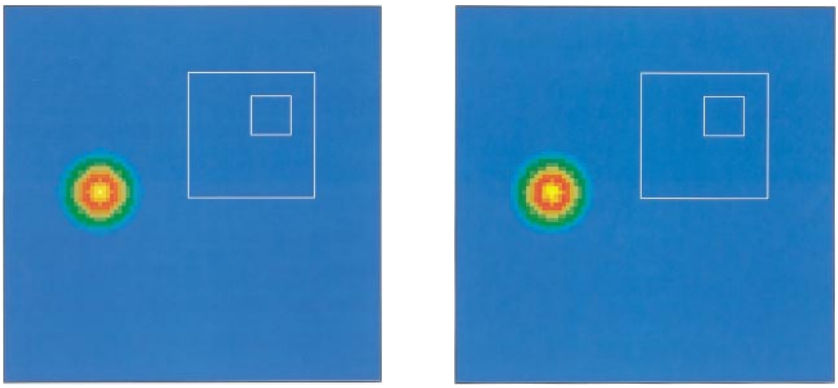

FIG. 4. Cone in the hemispheric domain, advection only—initial (left) before and final (right) after a full rotation.

solving the advection. The lower left part of the figures shows the rotation test for chemistry and advection combined. Sharp gradients from the chemistry can give rise to oscillations known as Gibbs phenomena and small oscillations can be seen in the surroundings of the cone. The oscillations are very small in this case, which show that the ASD method is very accurate, as can also be seen when peak values for the chemistry only set-up are compared with peak values for the advection plus chemistry set-up in Table II. The upper left part of the figures shows the rotation test carried out for the combination of chemistry, advection, and Forester filter. When the Forester filter is applied the small oscillations disappear (as seen in the minimum concentrations in Table II) and the result is very close to the result when chemistry only is applied.

7. TWO-WAY NESTING

Two nests are currently implemented in the model to obtain higher resolution over certain areas in the model domain using a two-way nesting method; see Fig. 1. The first nest covers the European area with a resolution of 50 km $\times$ 50 km. The second nest covers Denmark and close surroundings with a resolution of 16.67 km $\times$ 16.67 km.

The procedure for making the nested calculations is the same for the two nests. Every grid cell within the area to be nested in the coarse resolution (the mother domain) is

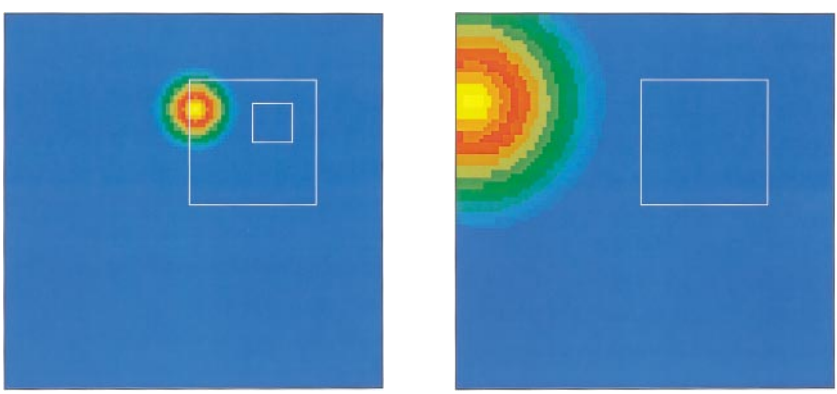

FIG. 5. Rotated cone in the hemispheric domain (left) and the first nest (right), advection only.

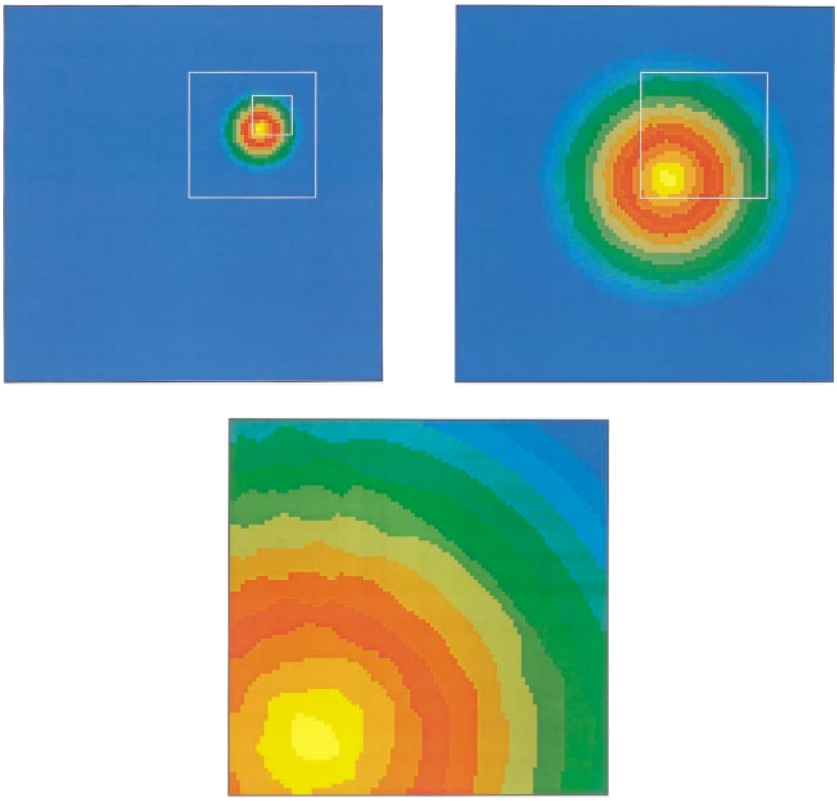

FIG. 6. Rotated cone in the hemispheric domain (upper left), the first (upper right), and the second nest (lower figure), advection only.

divided into nine new grid cells. The outermost two rows and columns of grid cells in the nested domain are given the values of the mother domain and they serve as the boundary rows and columns for the horizontal advection using the conditions as described in Section 4.4. Two-way nesting consists of nesting into the domains with higher resolution and nesting back out into the domains with coarser resolution. For the nesting from the coarse resolution domain to the higher resolution domain, C_{back}, as given in Eq. (33), is in the domain with higher resolution taken as the concentration in the respective grid in the mother domain; see Section 4.4. For the nesting back from the higher resolution domain to the coarser resolution domain, nine grid cells are averaged back to the coarser grid cell at the end of each calculation (mother domain time step) for all nested grids except the boundaries. The calculations of concentrations for the nested area are made in the higher resolution using a time step which is adjusted to the new spatial discretization using the CFL criterion.

To test the performance of the numerical method for solving advection when using a nested grid domain, the Molenkamp–Crowley rotation test has been used to advect a passive tracer through the domain including the two nests. The advection through a nested model domain is very complicated, when two-way nesting is applied. Retaining the maximum and the original shape of the cone after the nested area is exited puts very high demands on the numerical methods used to solve the advection. The result of the passive tracer rotation test can be seen in Figs. 4–6.

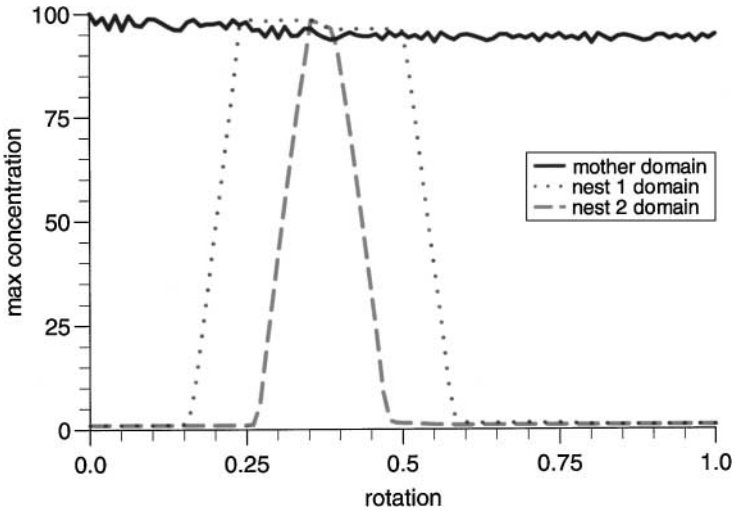

FIG. 7. Maximum value of the concentration distribution (peak of the cone) for the mother domain (solid line), the first nest (dotted line), and the second nest (dashed line).

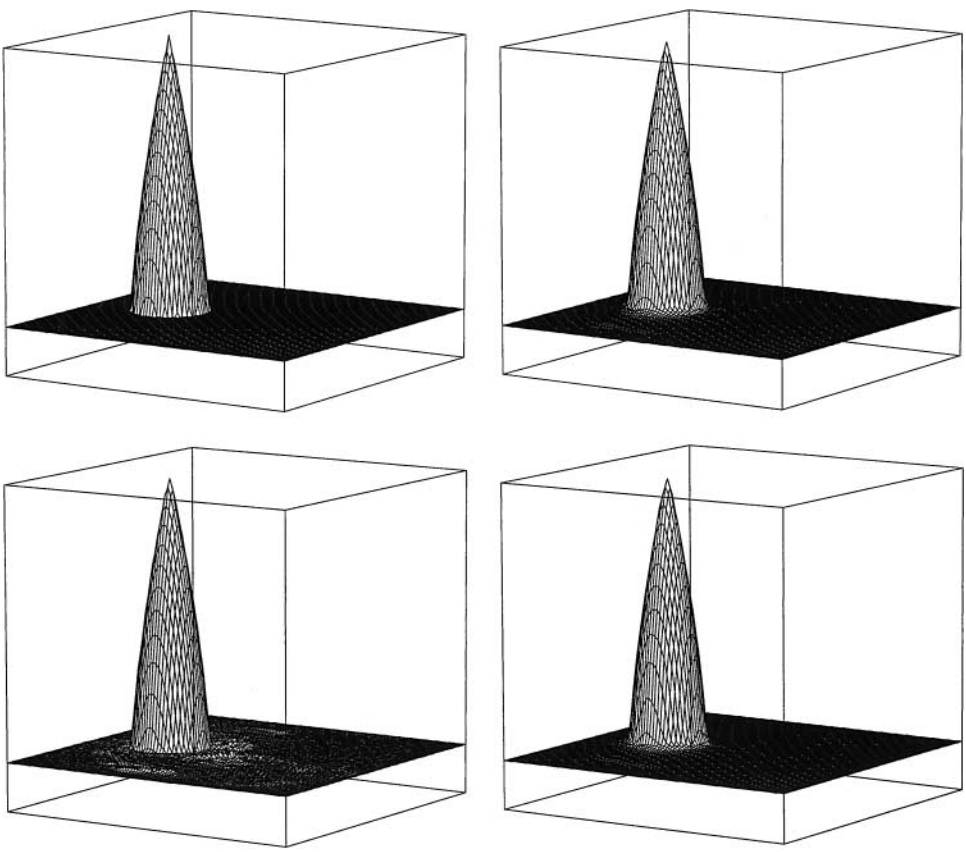

FIG. 8. Rotation test for NO_2 with nesting, rural conditions. The results are given for model runs with chemistry only (upper left), advection and chemistry combined with one nest (lower left), and advection, chemistry, and Forester filter combined with one nest (upper right). Furthermore model results are shown for advection, chemistry, and Forester filter combined with two nests (lower right).

Figure 4 shows the concentration cone of the passive tracer (as seen from above) before (left) and after (right) a full rotation. Note that the two nests in the rotation tests are not in the same position as in Fig. 1. This is done for technical reasons and has no influence on the results, since the topography of the northern hemisphere is not included in the rotation test. Figure 5 shows the cone after the first quarter of the rotation is completed. On the left the results in the entire model domain are seen, on the right the results in the first nest. Figure 6 shows the cone after approximately one third of the rotation is completed. The upper left shows the results in the mother domain, the upper right shows the results in the first nest, and the lower part of the figure shows the results in the second nest. Comparing the cone before and after the rotation through the nested area (Fig. 4) it can be seen that the shape of the cone is conserved to a large degree. The temporal evolution of the peak value of the cone as it passes through the nested domains can be seen in Fig. 7.

The solid line shows the peak value of the cone in the mother domain. There are small oscillations in the peak value, due to the spectral nature of the ASD method. In the nested domains the peak value is more stable due to the higher resolution, as can be seen from the dotted line (first nest) and the dashed line (second nest). Only approximately 5% of the maximum value is lost due to numerical diffusion during the rotation, indicating that the ASD method also works quite well for a nested grid model.

Finally rotation tests for combined advection and chemistry similar to tests described in Section 6 have been carried out for the model with one and two nests implemented, for both typical rural and urban conditions. The results for NO_2 and O_3 can be seen in Figs. 8 and 9 (typical rural concentration levels as input) and Figs. 10 and 11 (typical urban concentration levels as input). Values of maximum concentrations after one full rotation can be seen in Table III.

It can be seen that the nested area introduces small oscillations when Figs. 8 and 9 (lower left) are compared with Figs. 2 and 3 (lower left). In the upper right part of Figs. 8 and 9 and in Table III, it can be seen that the Forester filter to a large extent reduces the unwanted oscillations. The result of applying chemistry, advection, and Forester filter gives a

TABLE III

Maximum and Minimum Values of the Concentrations after One Full Rotation for the Model Set-Ups Chemistry Only, Advection Plus Chemistry, and Advection, Chemistry Plus Forester Filter

			Chemistry only		Advection, chemistry		Advection, chemistry, Forester	
Figure	Species	Nest	Max.	Min.	Max.	Min.	Max.	Min.
8	NO_2 r.	1	0.65	0.10	0.61	0.09	0.61	0.09
8	NO_2 r.	2	0.65	0.10	—	—	0.61	0.09
9	O_3 r.	1	134.00	30.86	129.92	29.64	129.92	30.45
9	O_3 r.	2	134.00	30.86	—	—	129.92	30.45
10	NO_2 u.	0	52.78	0.17	39.38	0.002	44.66	0.17
10	NO_2 u.	1	52.78	0.17	—	—	44.66	0.16
11	O_3 u.	0	60.90	10.56	56.84	16.24	56.84	14.62
11	O_3 u.	1	60.90	10.56	—	—	56.84	15.02

Notes. The initial concentrations correspond to rural (r) or urban (u) conditions. All values are in ppb.

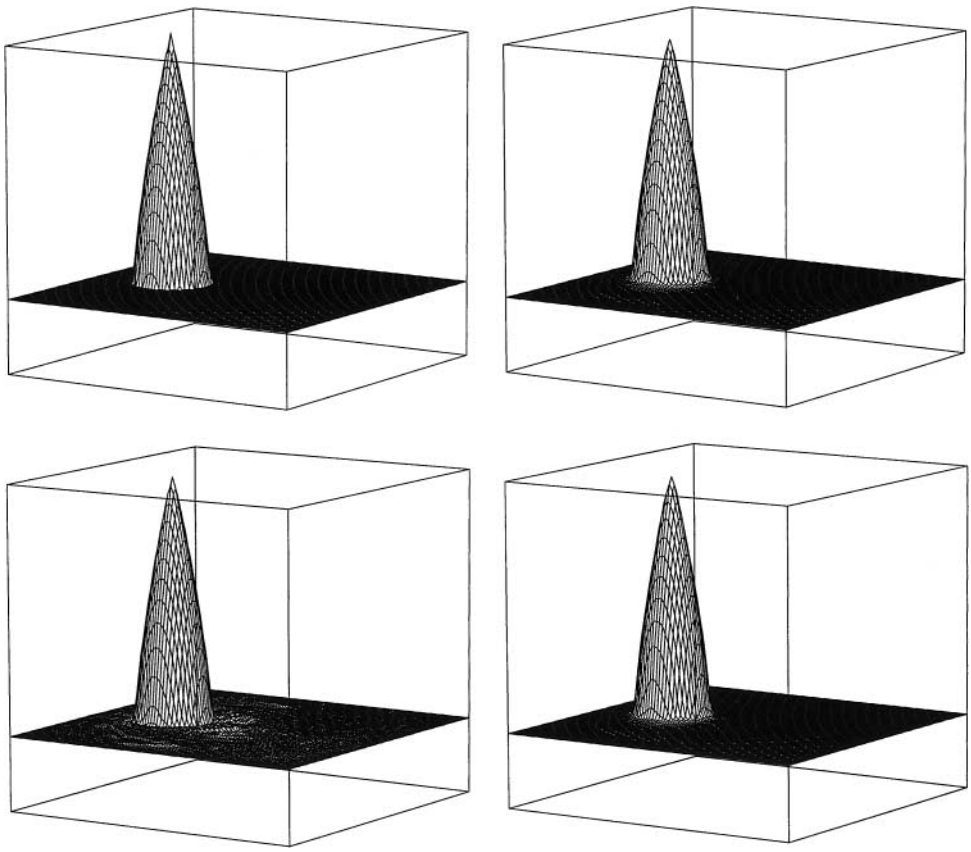

FIG. 9. Rotation test for O_3 with nesting, rural conditions. The results are given for model runs with chemistry only (upper left), advection and chemistry combined with one nest (lower left), and advection, chemistry, and Forester filter combined with one nest (upper right). Furthermore model results are shown for advection, chemistry, and Forester filter combined with two nests (lower right).

distribution, which is very close to the distribution obtained when chemistry only is applied, as it should be. Finally introducing yet another nest seems to be without difficulties as can be seen in Figs. 8 and 9 (lower right) and in Table III.

When initial concentrations typical for urban areas are applied to the rotation test, the coupling of NO_2 and O_3 can produce very sharp gradients in the O_3 distribution, because O_3 is depleted by high levels of NO_X. The results from performing the rotation test with urban concentration levels of NO_2 and O_3 can be seen in Figs. 10 and 11.

Comparing the result for NO_2 (Fig. 10) from applying advection and chemistry (upper right) with the same result in Fig. 2 (lower left), it can be seen that it is difficult to reproduce the maximum concentrations when using urban concentration levels as input, as is also clear when maximum concentrations are compared in Table III. Some small oscillations in the wake of the cone are also seen. These difficulties arise because of the sharper gradients in the concentration field under urban conditions. For O_3 the difficulties are even more pronounced (compare Fig. 11, upper right, with Fig. 3, lower left, as well as the minimum concentrations in Table III). The shape of the cone is changed dramatically due to the chemical interactions with nitrogen oxides, and this gives very sharp gradients especially around the edge of the cone. In Figs. 10 and 11 (lower left) the results of applying the Forester

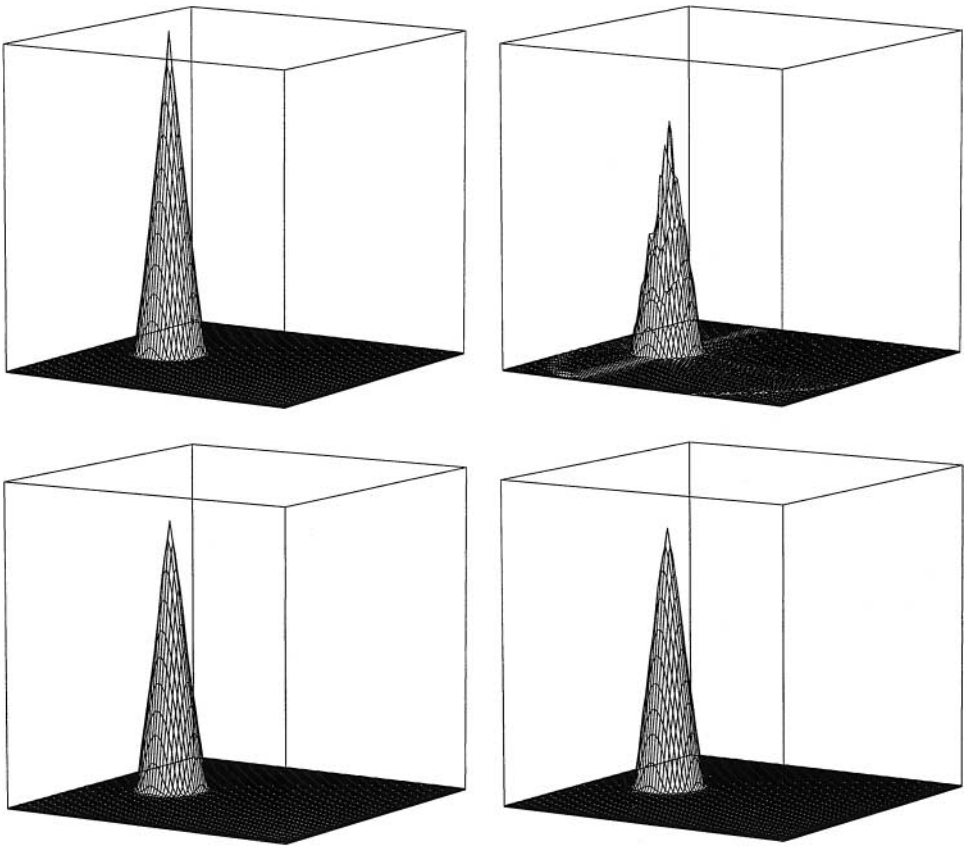

FIG. 10. Rotation test for NO_2 applying urban conditions. The results are given for model runs with chemistry only (upper left), advection and chemistry combined (upper right) and advection, chemistry, and Forester filter combined (lower left). Furthermore model results are shown for advection, chemistry, and Forester filter combined with one nest (lower right).

filter for NO_2 and O_3 respectively can be seen. Comparing with the results without Forester filter (upper right) the strength of the combination of the ASD method and the Forester filter is very visible. The oscillations introduced by the steep gradients are almost completely eliminated.

Finally in Figs. 10 and 11 (lower right) the result of performing the rotation test is shown for the model with advection, chemistry, and Forester filter, one nest, and urban concentration levels. As discussed earlier advection through a nested domain using two-way nesting is a very complicated task. The transport through the nested area is responsible for the small disturbances in the concentration distribution, especially distinct for O_3 in this case. However, maximum and minimum concentrations are still reproduced very nicely, as can be seen in Table III.

To investigate the oscillations in Figs. 10 and 11 more closely cross sections (for constant x value) through the center of the cone are provided in Figs. 12 and 13.

The cross sections in Figs. 12 and 13 correspond to the different rotation test results in Figs. 10 and 11, respectively. The solid line represents the chemistry only model set-up. The dark dotted lines represent cross sections of the cone resulting from running the rotation test with the advection and chemistry set-up (and no nesting). It is seen that the maximum

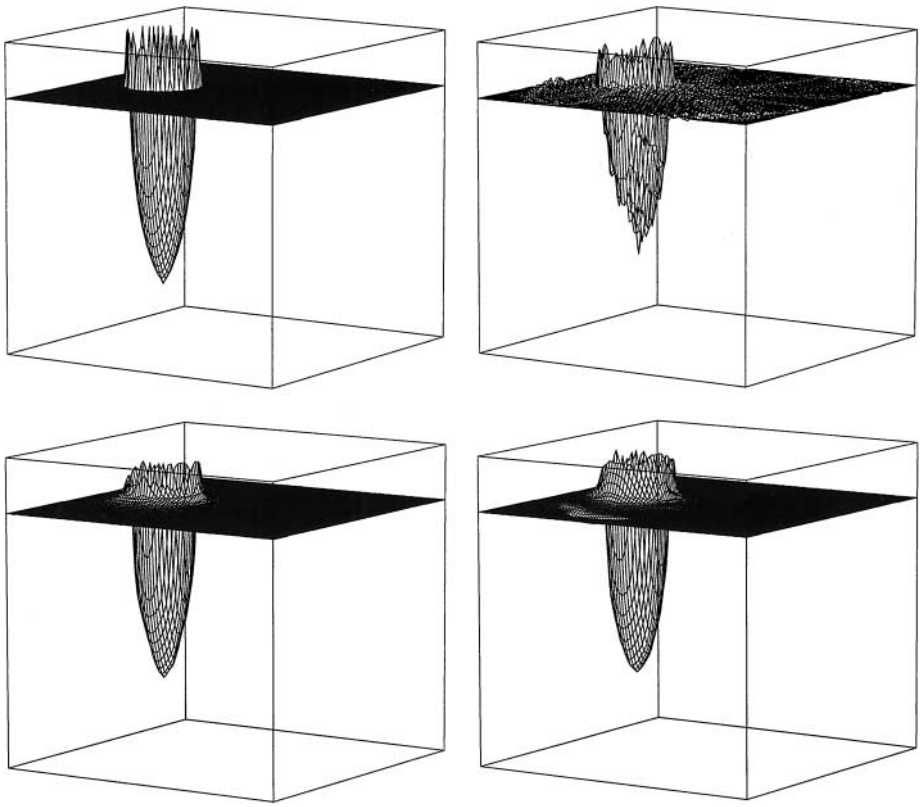

FIG. 11. Rotation test for O_3 with nesting, urban conditions. The results are given for model runs with chemistry only (upper left), advection and chemistry combined (upper right), and advection, chemistry, and Forester filter combined (lower left). Furthermore model results are shown for advection, chemistry, and Forester filter combined with one nest (lower right).

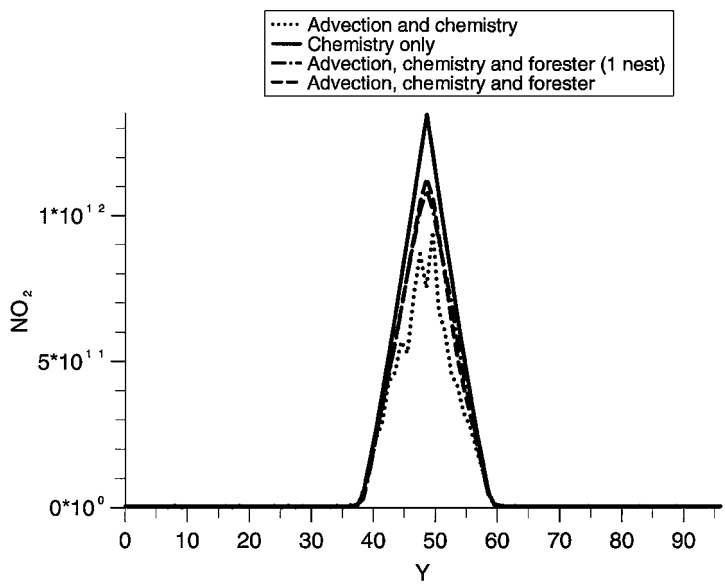

FIG. 12. Cross sections through the center of the NO_2 cones from Fig. 10, (constant x). The dark dotted line shows the advection and chemistry combination, solid line the chemistry only case, dashed line is advection, chemistry, and Forester filter combined, and light dotted line is advection, chemistry, and Forester filter and one nest.

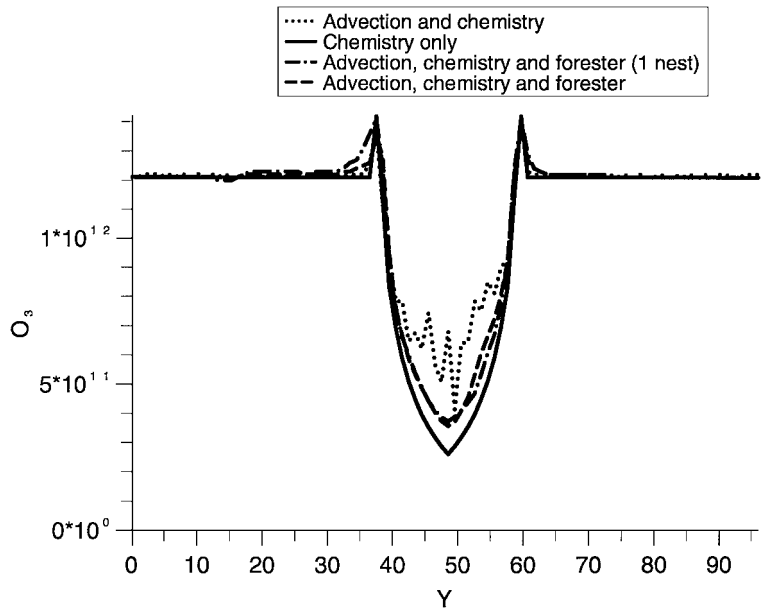

FIG. 13. Cross sections through the center of the O_3 cones from Fig. 11 (constant x). The dark dotted line shows the advection and chemistry combination, solid line the chemistry only case, dashed line is advection, chemistry, and Forester filter combined, and light dotted line is advection, chemistry, and Forester filter and one nest.

(NO_2) and the minimum (O_3) concentrations as well as the shape of the cone are difficult to reproduce in this set-up. When the Forester filter is applied (dashed line for no nesting, light dotted line for one nest), the shape of the cone is reproduced much more accurately, and the reproduction of the maximum and minimum concentrations is better.

8. CONCLUSIONS AND FUTURE WORK

A 3-D Eulerian nested air pollution model has been developed. The model domain covers the majority of the northern hemisphere and extends well up into the stratosphere. The numerical solution of the advection in the model is carried out using the method of accurate space derivatives. A new method for the calculation of the boundary conditions has been developed for the current implementation to account for nonperiodic boundary conditions. The numerical solution to the chemistry submodel is obtained by using a new implementation of the two-step method combined with the EBI method.

The numerical methods implemented in the model have been tested using the Molenkamp–Crowley rotation test. The test has been performed for the model with no nesting as well as with one and two nests and for both rural and urban conditions. The numerical test results look very promising. The combination of the ASD numerical method for solving advection and the Forester filter for diminishing effects of Gibbs phenomena works very well also for the nested grid domain and the error introduced by the advection is small.

The results of the rotation test with no nesting show almost no difference between applying chemistry only and applying advection, chemistry and Forester filter combined. This shows

that the numerical solution works as expected. The numerical solution of advection only for the nested model domain has been tested by rotating a passive tracer. Almost no difference in the distribution of the tracer (maximum is preserved within 5%) is observed after one rotation. This shows that the ASD method with the new boundary conditions is capable of solving the advection in nested domains accurately.

The results of the rotation test of the model with one and two nests show that small oscillations are introduced when chemistry and advection combined for one nest is applied, especially when urban concentration levels are used as input. However, these oscillations are almost completely removed by the Forester filter. The results of the rotation test with advection, chemistry, and Forester filter combined for the model with two nests are very good.

When very high resolutions are approached, not only the performance of the numerical methods, but also equally important the description of physical processes needs to be reconsidered. The validity of all basic physical assumptions underlying the mathematical formulation of the model must be reevaluated.

The current development in available computer power makes it possible to extend an air pollution transport model to finer and finer resolution. However, the accuracy of the model does not necessarily increase with the resolution. The performance of the model depends on several factors concerning the applied parameterizations, the description of chemistry, the model scale, the quality of the input data, such as emissions inventories and land use data, the accuracy and resolution of the meteorological data, and the numerical methods used as well as the initial and boundary conditions.

In the further development of the REGINA model, we will examine how to optimally combine all these factors to reach a desired level of performance, e.g., defined by allowable environmental effects (damages). When completed, REGINA will be contributing to the Danish Background Monitoring Programme and it will be included in the THOR system for operational air pollution forecasting (see [8, 9] for details).

ACKNOWLEDGMENTS

The Danish Research Academy and the Risø National Laboratory are greatly acknowledged for partial funding of the work presented in this paper.

REFERENCES

1. R. Atkinson, D. L. Baulch, R. A. Cox, R. F. Hampson, Jr., J. A. Kerr, and J. Troe, Evaluated kinetic and photochemical data for atmospheric chemistry: Supplement III, *J. Phys. Chem. Ref. Data* **18**, 881 (1989).
2. J. Bartnicki, A simple filtering procedure for removing negative values from numerical solutions of the advection equation, *Environment. Software* **4**(4), 187 (1989).
3. J. Bartnicki, K. Olendrzynski, K. Abert, P. Seibert, and B. Morariu, Numerical approximation of the transport equation: Comparison of five positive definite algorithms, *International Institute for Applied Systems Analysis, Laxenburg, Austria, WP-90-10* (1990).
4. J. G. Blom and J. G. Verwer, A comparison of integration methods for atmospheric transport–chemistry problems, *J. Comput. Appl. Math.* **126**, 381 (2000).
5. J. Brandt, J. Wasniewski, and Z. Zlatev, Handling the chemical part in large air pollution models, *Appl. Math. Comput. Sci.* **6**(2), 331 (1996).
6. J. Brandt, I. Dimov, K. Georgiev, J. Wasniewski, and Z. Zlatev, Coupling the advection and the chemical parts of large air pollution models, in *Proceedings of the Third International Workshop, "PARA'96" at UNI-C, Lyngby, Denmark, August 18–24, 1996*, Lecture Notes in Computer Science. Applied Parallel Computing,

Industrial Computation and Optimisation, edited by J. Wasniewski, J. Dongarra, K. Madsen, and D. Olesen, (Springer-Verlag, Berlin, 1997), Vol. 1184, p. 18.

7. J. Brandt, A. Bastrup-Birk, J. H. Christensen, T. Mikkelsen, S. Thykier-Nielsen, and Z. Zlatev, Testing the importance of accurate meteorological input fields and parameterizations in atmospheric transport modelling using DREAM—Validation against ETEX-1, *Atmospher. Environment* **32**(24), 4167 (1998).
8. J. Brandt, J. H. Christensen, L. M. Frohn, R. Berkowicz, and Z. Zlatev, Optimization of operational air pollution forecast modeling from European to local scale, in *Proceedings from the 3rd GLOREAM workshop, Napoli, Italy, September 22–24, 1999*.
9. J. Brandt, J. H. Christensen, L. M. Frohn, F. Palmgren, R. Berkowicz, and Z. Zlatev, Operational air pollution forecasts from European to local scale, *Atmospher. Environment* **35**(1), 91 (2001).
10. A. Bott, A positive definite advection scheme obtained by non-linear renormalization of the advective fluxes, *Month. Weather Rev.* **117**, 1006 (1989).
11. A. Bott, Monotone flux limitations in the area preserving flux-form advection algorithm, *Month. Weather Rev.* **120**, 2593 (1992).
12. J. S. Chang, R. A. Brost, I. S. A. Isaksen, S. Madronich, P. Middleton, W. R. Stockwell, and C. J. Walcek, A three-dimensional Eulerian acid deposition model: Physical concepts and formulation, *J. Geophys. Res.* **92**, 14,681 (1987).
13. J. S. Chang, P. B. Middleton, W. R. Stockwell, C. J. Walcek, J. E. Pleim, H. H. Lansford, F. S. Binkowski, N. L. Seaman, J. N. McHenry, S. Madronich, P. J. Samson, and H. Hash, The regional acid deposition model and engineering model, in *Acid Deposition: State of Science and Technology*, *Report* **4** (Emissions, Atmospheric Processes and Deposition, National Acid Precipitation Programme, 1990), Vol. 1.
14. D. P. Chock, A comparison of numerical methods for solving the advection equation-III, *Atmospher. Environment* **A 25**(5–6), 853 (1991).
15. D. P. Chock and S. L. Winkler, A comparison of advection algorithms coupled with chemistry, *Atmospher. Environment* **28**(16), 2659 (1994).
16. J. H. Christensen, Testing advection schemes in a three-dimensional air pollution model, *J. Math. Comput. Model.* **18**(2), 75 (1993).
17. J. H. Christensen, The Danish eulerian hemispheric model—A three-dimensional air pollution model used for the Arctic, *Atmospher. Environment* **31**(24), 4169 (1997).
18. W. P. Crowley, Numerical advection experiments, *Month. Weather Rev.* **96**, 1 (1968).
19. D. Dabdub and J. H. Seinfeld, Numerical advective schemes used in air quality models—Sequential and parallel implementation, *Atmospher. Environment* **28**(20), 3369 (1994).
20. W. B. DeMore, D. M. Golden, R. F. Hampson, C. J. Howard, C. Kolb, M. J. Kurylo, M. J. Molina, A. R. Ravishankara, and S. P. Sander, Chemical kinetics and photochemical data for use in stratospheric modeling, in *JPL Publications* (NASA Jet Propulsion Laboratory, California Institute of Technology, Pasadena, California, 1992), Vol. 90–20.
21. F. Flatøy, Balanced wind in advanced advection schemes when species with long lifetimes are transported, *Atmospher. Environment, Part A* **27**(12), 1809 (1993).
22. F. Flatøy, Ø. Hov, and H. Smit, Three-dimensional model studies of exchange processes of ozone in the troposphere over Europe, *J. Geophys. Res.* **100**(D6), 11,465 (1995).
23. F. Flatøy, Ø. Hov, C. Gerbig, and S. J. Oltmansm, Model studies of the meteorology and chemical composition of the troposphere over the North Atlantic Dutin, August 18–30, 1993, *J. Geophys. Res.* **101**, 29,317 (1996).
24. C. K. Forester, Higher order monotonic convective difference schemes, *J. Comput. Phys.* **23**, 1 (1977).
25. J. Gazdag, Numerical convective schemes based on accurate computation of space derivatives, *J. Comput. Phys.* **13**, 100 (1973).
26. G. A. Grell, J. Dudhia, and D. R. Stauffer, *A Description of the Fifth-Generation Penn State/NCAR Mesoscale Model (MM5), Mesoscale and Microscale Meteorology Division, National Center for Atmospheric Research, Boulder, Colorado, NCAR Technical Note*, NCAR/TN-398 + STR (1995).
27. H. Hass, Description of the EURAD Chemistry–Transport Model, Version 2 (CTM2), in *Mitteilungen aus dem Institut fur Geophysik und Meteorologie der Universitat Zu Koln*, edited by A. Ebel, F. M. Neubauer, and P. Speth, No. 83 (1991).

28. O. Hertel, R. Berkowicz, J. H. Christensen, and Ø. Hov, Test of two numerical schemes for use in atmospheric transport–chemistry models, *Atmospher. Environment* **27A**(16), 2591 (1993).
29. O. Hertel, J. H. Christensen, E. H. Runge, W. A. H. Asman, R. Berkowicz, M. F. Hovmand, and Ø. Hov, Development and testing of a new variable scale air pollution model—ACDEP, *Atmospher. Environment* **29**(20), 1267 (1995).
30. E. V. Holm, *High-order Numerical Methods for Advection in Atmospheric Models*, Ph.D. thesis (Stockholm University, Department of Meteorology, 1994).
31. Ø. Hov, Z. Zlatev, R. Berkowicz, A. Eliassen, and L. P. Prahm, Comparison of numerical techniques for use in air pollution models with non-linear chemical reactions, *Atmospher. Environment* **23**(5), 967 (1989).
32. J. E. Jonson and I. S. A. Isaksen, *The Impact of Solar Flux Variation on the Tropospheric Ozone Chemistry*, Report 81 (Institute of Geophysics, University of Oslo, 1991).
33. J. D. Lambert, *Numerical Methods for Ordinary Differential Systems: The Initial Value Problem* (Wiley, Chichester, 1991).
34. J. Langner, R. Bergstrom, and K. Pleijel, European scale modeling of sulphur, oxidised nitrogen and photochemical oxidants: Model development and evaluation for the 1994 growing season, in *SMHI RMK* (Swedish Meteorological and Hydrological Institute, 1998), No. 82.
35. D. Lanser and J. G. Verwer, Analysis of operator splitting for advection–diffusion-reaction problems from air pollution modeling, *J. Comput. Appl. Math.* **111**, 201 (1999).
36. E. C. McDonald-Buller, H. M. Liljestrand, and K. Sepehrnoori, Numerical modeling of dry deposition coupled to 22 photochemical reactions, *Atmospher. Environment* **33**, 1491 (1999).
37. G. J. McRae, W. R. Goodin, and J. H. Seinfeld, Numerical solution of the atmospheric diffusion equations for chemically reacting flows, *J. Comput. Phys.* **45**, 1 (1984).
38. L. Menut, R. Vautard, M. Beekmann, and C. Honore, Sensitivity of photochemical pollution using the adjoint of a simplified chemistry–transport model, *J. Geophys. Res.* **105**(D12), 15,379 (2000).
39. C. R. Molenkamp, Accuracy of finite-difference methods applied to the advection equation, *J. Appl. Meteorol.* **7**, 160 (1968).
40. D. W. Pepper, C. D. Kern, and P. E. Long, Jr., Modeling the dispersion of atmospheric pollution using cubic splines and chapeau functions, *Atmospher. Environment* **13**, 223 (1979).
41. E. Reimer, G. Wiegand, J. Flemming, M. Dlabka, W. Enke, K. Berendorf, W. Weiss, and R. Stern, *Erstellung einer Osone-Kursfristprognose fur das Smogfruhwarnssystem*, Abschlussbericht des UBA F & E Vorhabens 29543817 (Berlin, 2000).
42. L. Robertson, J. Langner, and M. Engardt, An Eulerian limited-area atmospheric transport model, *J. Appl. Meteorol.* **38**, 190 (1999).
43. Sai, *Users Guide to the Variable-Grid Urban Airshed Model (UAM-V)*, SYSAPP-95/027, (Systems Applications International, San Rafael, California, 1995).
44. B. Sportisse, An analysis of operator splitting techniques in the stiff case, *J. Comput. Phys.* **161**, 140 (2000).
45. R. Stern, *Entwicklung und Anwendung eines dreidimensionalen photochemischen Ausbreitungsmodells mit verschiedenen chemischen Mechanismen* (Freie Universitat Berlin, 1994).
46. A. Strand and Ø. Hov, A 2-dimensional global study of tropospheric ozone production, *J. Geophys. Res. A* **99**(D11), 22,877 (1994).
47. S. A. Tomlin, S. Ghorai, G. Hart, and M. Berzins, 3D adaptive unstructured meshes for air pollution modelling, *Environment. Management Health* **10**(4), 267 (1999).
48. J. G. Verwer, J. G. Blom, M. Van Loon, and E. J. Spee, A comparison of stiff ODE solvers for atmospheric chemistry problems, *Atmospher. Environment* **30**(1), 49 (1996).
49. Z. Zlatev, *Computer Treatment of Large Air Pollution Models*, Environmental Science and Technology Library, Vol. 2. (Kluwer Academic, Dordrecht/Norwell, MA, 1995).